Heliyon 10 (2024) e34301

Contents lists available at ScienceDirect

Heliyon

journal homepage: www.cell.com/heliyon

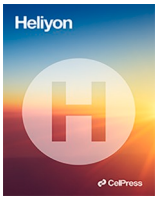

Research article

An engineered lactate oxidase based electrochemical sensor for continuous detection of biomarker lactic acid in human sweat and serum

Qingrong He [a,2], Cheng Wang [a,2], Rohit Jain [b,c,d,2], James Byrnes [e], Erik R. Farquhar [b,d], Elliot Reed [b,f], Elizabeth Berezovsky [b,f], Mark R. Chance [b,c,d,f], David Lodowski [b,c,f,1], Ran An [a,b,g,1,*]

[a] *Department of Biomedical Engineering, University of Houston, United States*
[b] *Biomolecular Structure and Integration of Sensors (BioSIS) Program, Department of Nutrition, School of Medicine, Case Western Reserve University, United States*
[c] *Center for Proteomics and Bioinformatics, School of Medicine, Case Western Reserve University, United States*
[d] *Center for Synchrotron Biosciences, School of Medicine, Case Western Reserve University, United States*
[e] *National Synchrotron Light Source II, Brookhaven National Laboratory, United States*
[f] *Sensate Biosystems LLC, Cleveland, OH, United States*
[g] *Department of Biomedical Sciences, University of Houston, United States*

A B S T R A C T

Lactate levels in humans reveal intensity and duration of exertion and provide a critical readout for the severity of life-threatening illnesses such as pediatric sepsis. Using the lactate oxidase enzyme (Lox) from *Aerococcus viridians*, we demonstrated its functionality for lactate electrochemical sensing in physiological fluids in a lab setting. The structure and dynamics of LOx were validated by crystallography, X-ray scattering, and hydroxyl radical protein footprinting. This provided a validated protein template for understanding and designing an enzyme-based electrochemical sensing elements. Using this template, LOx enzyme variants were generated and compared. Comparison of the variants demonstrates that one exhibits effective lactate sensing at significantly reduced operating voltages. Additionally, we demonstrate that the four hexahistidine-tags on each enzyme tetramer are sufficient for immobilization to create a durable, functional sensor, with no need for a covalent attachment, enabling self-immobilization and eliminating the need for additional immobilization steps. The functionality of the LOx enzyme variants was verified at physiological lactate concentrations in both human serum (0–4 mM) and artificial sweat (0–100 mM) using 3-electrode setups for analysis of the three variants in parallel. Accuracy of measurement in both artificial sweat and human serum were high. Employing a microfluidic flow cell, we successfully monitored varying lactate levels in physiological fluids continuously over a 2h period. Overall, this optimized LOx enzyme, which self-immobilizes onto gold sensing electrodes, facilitates efficient and reliable lactate detection and continuous monitoring at reduced operating voltages suitable for further development towards commercial use.

1. Introduction

Lactate (l-lactate or lactic acid) is produced from pyruvate by lactate dehydrogenase during normal and abnormal metabolism and is directly related to levels of metabolic exertion during exercise and training [1,2]. In addition, lactate accumulation in humans can

* Corresponding author. Department of Biomedical Engineering, University of Houston, United States.
E-mail addresses: lodowski@gmail.com (D. Lodowski), ran@uh.edu (R. An).
[1] Joint Correspondence.
[2] Indicates equal contributions.

https://doi.org/10.1016/j.heliyon.2024.e34301
Received 24 June 2024; Accepted 8 July 2024
Available online 9 July 2024

occur due to numerous medical conditions including heart disease, sepsis, and diabetes [3]. This over-accumulation of lactate can lead to clinical complications including pain, muscle fatigue, pH imbalance, impaired muscle/limb performance, respiratory changes, cardiovascular stress, and organ failure [4,5]. In clinical settings, lactate levels serve as a key biomarker for detecting sepsis, monitoring heart failure, assessing the severity of shock, and identifying metabolic acidosis, aiding in the early diagnosis and treatment of these conditions [6]. In athletics, lactate levels serve as a key biomarker for gauging performance, fine-tuning training regimens, assessing muscle fatigue, and ensuring safe training practices [7]. Currently, lactate measurement is predominantly conducted discontinuously in centralized laboratories. There are limited technologies available that facilitate lactate detection at the point of care (POC), and these technologies typically allow for intermittent detection, rather than continuous monitoring [8,9] and require a fresh blood draw for each measure. Continuous monitoring of lactate in a POC setting offers significant benefits in predicting and managing disorders associated with lactate imbalances, as well as providing valuable insights to optimize athletic performance and training regimes [10,11].

Enzymatic electrochemical sensors utilizing lactate oxidase (LOx) offer rapid, sensitive, and selective lactate measurement, which is ideal for precise and continuous lactate monitoring [12,13]. In these sensors, lactate is enzymatically oxidized by LOx to produce pyruvate and hydrogen peroxide (H_2O_2) [14]. Then, the hydrogen peroxide is catalytically decomposed on the electrode surface to produce oxygen gas (O_2), water (H_2O), and electrons ($2e^-$) [15]. The sensing electrode quantitatively determines H_2O_2 levels by monitoring these generated electrons, consequently inferring the concentration of lactate [16].

Despite advancements in the development of lactate electrochemical sensors, considerable challenges persist in the commercialization of LOx-based electrochemical sensors. Detecting lactate using wildtype LOx without any electron mediator requires a relatively high potential (0.6 V vs. standard Ag/AgCl in phosphate buffer saline (PBS), and ~0.65–0.8 V in sweat) [5,17]. This elevated potential often results in non-specific or spontaneous electrochemical reactions, which in turn produce interfering signals and amplify noise, hindering sensor effectiveness and reliability [18,19]. Additionally, high voltage in enzymatic sensors can cause electrode fouling, characterized by the oxidative degradation of conductive materials, deactivation/loss of enzyme, and contamination due to the adhesion of proteins or peptides [20,21]. Most sensors employ a mediator in the composition of the working electrode such as Prussian Blue, tetrathiafulvalene (TTF), and phenazine ethosulfate (PES) [15,22,23] in order to lower the sensor operation voltage [15,22,23]. However, Prussian blue and TTF suffer from low solubility and complex synthesis processes, potentially posing difficulties for large-scale commercial production of LOx sensors. Phenazine has been established as an innovative electron mediator, and the use of phenazine-modified lactate oxidase has been shown to facilitate efficient lactate sensing [15] ostensibly by enabling a quasi-direct electron sensing modality. Although phenazine-modified lactate oxidase has demonstrated feasibility in lactate detection, its functionality has only been demonstrated in PBS solutions rather than actual biofluids [15]. Additionally, these previous studies only demonstrated a limited range of linearity up to 5 mM for measured current against lactate concentration in PBS [15], whereas the physiological lactate concentrations in sweat fall between 5 and 25 mM and can escalate to 43.7 mM during endurance exercise and can peak at 115.8 mM in scenarios of exhaustive exercise [24,25]. Moreover, the selective lactate sensing using phenazine-modified lactate oxidase required the application of a negative voltage [15]. These negative voltages are known to cause cathodic reduction of dissolved oxygen molecules, which may potentially generate currents that interfere with accurate lactate detection [26–28].

Besides the relatively high operating voltage requirement, immobilizing the LOx enzyme on sensing electrodes requires specific techniques [29,30]. Various approaches to immobilization including entrapment in polymeric membranes [31–33], covalent immobilization [34], confinement inside so-gel matrix [31], and cross-linking [35] have been developed to assist LOx enzyme immobilization on electrode surfaces with materials including gold, graphene, platinum, and other materials [36–38]. However, these methods involve advanced biosensors composed with nanoparticles [39], nanotubes [40], gels [31], or involvement with additional chemical treatment during sensor fabrication [41]. As a result, this complexity not only complicates the manufacturing timeline and escalates production costs but also demands enhanced quality control measures.

To address these challenges, we characterized engineered variants of LOx enzyme from *Aerococcus viridians* for their viability as sensors under physiologically relevant ranges of lactate. The location of the hexahistidine affinity tag on these engineered LOx enzymes allows self-immobilization onto gold electrodes absent any covalent coupling steps. Additionally, when modified with phenazine, these LOx enzymes demonstrate their electrochemical sensing reactivity with lactate at reduced voltages in serum and sweat, providing an increased range of linearity across physiological lactate levels. We first expressed and purified recombinant LOx, followed by determining its atomic structure by xra-crystallography. We also characterized the LOx oligomeric state and interactions with lactate using small-angle X-ray scattering and hydroxyl radical protein footprinting techniques. The recombinant LOx enzyme was modified by altering two amino acids, A96L to reduce unnecessary oxygen transfer and N212K to allow covalent attachment of a phenazine ethosulfate molecule near the FMN cofactor for quasi-direct electron transfer to the electrode. A hexahistidine tag was also appended to all constructs to simplify purification {Hiraka, 2020 #45}. This allowed the comparison of three variants, v1-v3, representing wild type, mutant, and mutant with phenazine attached, respectively. Interestingly, the v3 (phenazine modified) variant shows effective lactate sensing at significantly reduced operating voltages at 0.29 V vs standard Ag/AgCl in human serum and 0.59 V vs. standard Ag/AgCl in artificial sweat. The functionality of LOx enzyme variants was explored at physiological lactate concentrations in both human serum (0–4 mM) and artificial sweat (0–100 mM) using 3-electrode setups to monitor variants in parallel. We further demonstrated continuous monitoring of variable lactate concentrations over 2-h with a flow-cell setup. These developments form the basis for further development toward commercial applications of the technology.

2. Materials and methods

2.1. Chemicals and materials

The sodium salt of L-lactate ($C_3H_5NaO_3$) was purchased from Sigma-Aldrich (MO, USA). The commercial LOx was purchased from Sigma-Aldrich (MO, USA). Dulbecco's Phosphate Buffered Saline (PBS) were obtained from Avantor (PA, USA). Amine Reactive Electron Mediator (arPES) was obtained from Dojindo molecular technologies (Gaithersburg, MD). The screen-printed electrodes (SPE) DRP-220AT (Metrohm, DropSens DRP-220AT, Working electrode: Gold, 12.56 mm^2, Reference electrode: Ag/AgCl, Counter electrode: Gold) were obtained from Metrohm DropSens (Girona, Spain). Ag/AgCl reference electrode (part number: CHI111; CH Instruments, Inc.) and Platinum Wire Counter Electrode (part number: CHI115) from Chinstruments (TX, USA). A Palmsens4 electrochemical work station was purchased from Palmsens BV (Enschede, Netherlands). All chemicals were reagent grade. Bacterial expression constructs for *Aerococcus viridians* LOx expression were designed in silico and synthesized and obtained from ATUM biotechnology (San Francisco, CA, USA).

2.2. LOx expression and purification

A synthetic vector construct consisting of a codon-optimized, N-terminally His-tagged *Aerococcus viridians* LOx construct was designed and synthesized (ATUM Bio, Newark, CA). *E. coli (BL21 (DE3)(pLysS))* were transformed with this vector and grown at 37 °C with shaking to an OD600 of 0.65 in a modified terrific broth mixture supplemented to 1 mM $MgCl_2$, 0.5 % glucose and 1.0 % glycerol; upon achieving this value they were induced for 4 h with 1 mM IPTG. Induced cells were harvested by centrifugation and frozen at −80 °C until purification. In a typical purification, 12 L of frozen cells were grounded under liquid nitrogen in a mortar and pestled to a fine powder prior to thawing by dilution in Lysis buffer (20 mM HEPES pH 7.5, 100 mM NaCl) supplemented with 0.5 mg/g cell paste of Lysozyme, 2 EDTA free protease inhibitor tablets (Roche) and Benzonase to reduce sample viscosity. Cells were passed twice through a microfluidizer for lysis (typically at > 10,000 PSI). Supernatant was harvested by centrifugation (35,000×*g*, 30 min) to gather the supernatant containing LOx. Supernatant was loaded onto a 5 ml Ni-NTA superflow column at 2 mL/min, column was washed with 50 mL of high salt wash (20 mM HEPES 7.5, 300 mM NaCl, 10 mM imidazole), followed by 5 column volumes of low salt wash (20 mM HEPES 7.5, 100 mM NaCl, 10 mM imidazole). LOx was then eluted from the column with elution buffer (20 mM HEPES 8.2, 100 mM NaCl, 300 mM imidazole) and 1 mL fractions were collected. The elution fractions were analyzed by SDS-PAGE to check for protein quantity and purity. Fractions that exhibited LOx of high purity were pooled and concentrated to 10–15 mg/mL in an Amicon Ultra 100 kDa MWCO concentrator and further purified using gel filtration chromatography using 20 mM HEPES pH 7.5, 100 mM NaCl buffer to remove imidazole and low molecular weight impurities. Protein purity was assessed by SDS-PAGE and high purity (typically 95 %) fractions were pooled and concentrated in an Amicon Ultra 15,100 kDa MWCO concentrator to a final concentration of 16–20 mg/mL. Pure LOx was frozen as 50 μL drops in liquid nitrogen and stored until further use. Purified LOx was buffer exchanged three times into PBS prior to hydroxyl footprinting to remove HEPES buffer. All concentrations were assessed with A_{280} measurements in a NanoDrop using an extinction coefficient of 205,360 $M^{-1}cm^{-1}$ for the tetrameric Lox assembly due to the nonstandard distribution of aromatic residues in the LOx sequence.

2.3. LOx small and Wide-angle X-ray scattering (SAXS/WAXS)

SAXS/WAXS data was collected simultaneously at the Life Sciences X-ray beamline (LiX) at NSLS-II. Samples were prepared and shipped to NSLS-II and measured using the Size Exclusion Chromatography coupled with SAXS (SEC-SAXS) setup at LiX. Briefly, 60 μL of sample was injected into a Superdex 200 Increase 5/150 GL column (Cytiva) using an Agilent 1260 Infinity II Bio Inert HPLC system and multisampler. Details of the experimental setup and mail-in procedure can be found here [42,43].

The column was equilibrated in several column volumes of 1 × PBS at a flow rate of 0.35 mL/min. SAXS/WAXS data were simultaneously collected on a Pilatus 1 M and Pilatus 900K respectively, with a 2 s exposure time. Detector images were merged, scaled and peak regions were determined using beamline specific software, py4xs (https://github.com/NSLS-II-LIX/py4xs.git) and lixtools (https://github.com/NSLS-II-LIX/lixtools.git). Guinier fitting, Kratky generation, P(r) function were performed using GNOM [44].

Bead model construction employed DAMMIF and alignment with the crystal structure was performed with SUPCOMB and visualized using PyMOL (The PyMOL Molecular Graphics System, Version 2.0 Schrödinger, LLC).

2.4. LOx crystallization, X-ray data collection and structure determination

Initial crystallization studies were conducted utilizing a variety of commercial sparse matrix screen as well as screens designed around prior LOx crystallization conditions. Initial crystals were observed at a variety of pH values ranging from 4 to 7.5 and a large range of Ethylene glycol concentrations (15–40 %) as the precipitant. Optimal crystal conditions were found to be 30 % Ethylene glycol, 100 mM Citrate pH 5.5, 50 mM NaCl and 100 mM sodium lactate (pH adjusted to pH 5.5). Crystals were grown in VDX sitting drop plates with a well volume of 500 μL and 2 μL purified protein, 2 μL well solution and 20 μL 18.3 MΩ water at 18 °C. Crystals appeared after 3–4 days and grew to maximum size over 2–3 weeks. Crystals were harvested and cryoprotected by transfer into perfluoropolyether Cryo oil (Hampton Research) in appropriately sized microloops (Mitegen), and frozen in and stored in Unipucks (CPS, Inc) under liquid Nitrogen until data collection.

Data collection was performed at the Advanced Photon Source, 19-ID-C beamline as well as at the AMX beamline at NSLS-II. The

ability to switch to a short wavelength and move the large format detector close to sample was essential to obtaining high resolution diffraction data. Initial snapshots separated by 90° were employed to determine optimal starting point and rotational range. Data were collected utilizing the vector translation strategy to optimize fresh crystal exposure and maximize dose/minimize damage to crystals. We utilized a wavelength of 0.7293 Å, as well as a sample to crystal distance of 100 mm to minimize spot spacing enabling capture of high angle reflections.

Data were processed with a pipeline approach using DIALS for initial data reduction and pointless/aimless for scaling and assignment of R_{free}. An initial model was solved by molecular replacement using PHASER, and then model was initially completed using ARP/WARP. Model was examined and rebuilt by hand in COOT and refined using PHENIX_refine, with more than 20 full model building and refinement iterations. During model building, we omitted the loop between residues 205 and 220, and rebuilt into the resultant Fo-Fc density maps. Despite this approach, there was a significantly poor RSCC for this region, perhaps explaining the variability of this region in multiple prior PDB deposits. Ultimately, we decided to remove these residues in the deposited structure (PDB: 8UFY) to reflect this structural variability; it should be noted that this region has little concordance amongst previously determined structures further supporting the assessment of its structural dynamics.

2.5. LOx X-ray footprinting, mass spectrometry sample preparation and data analysis

A sample containing 2 μM LOx (0.3 mg/ml) in 1 × PBS (pH 7.4) was first reconstituted with Alexa488 dye (to a final Alexa488 concentration of 4 μM) in free form and with 800 μM lactate for determining appropriate X-ray dosage. Based on Alexa488 dose response assay results, X-ray fluxes corresponding to different beam powers (at 400 mA NSLS-II ring current) were tuned by changing aluminum thickness attenuation at exposure times of 0 ms, 12 ms, 20 ms, and 30 ms. Samples for Alexa488 dose response and mass spectrometry analysis were exposed in 5 μL volumes in 200 μL PCR tubes, with 8 replicates for each sample and exposure condition using a 96-well high-throughput apparatus and a plate reader for Alexa488 fluorescence readout [45,46].

Following X-ray exposures, samples were immediately quenched with methionine amide to a final concentration of 10 mM, frozen in liquid nitrogen, shipped on dry ice to CWRU for mass spectrometric analysis, and stored at −80 °C. Frozen hydroxyl labeled LOx samples were retrieved from −80 °C storage and thawed on ice, with four aliquots (~6.7 μg) mixed for each exposure condition. LOx samples were prepared for protease digestion at 1.6 M urea, 20 mM Tris pH 8.5 concentrations by reconstitution with 8 M urea and 100 mM Tris pH 8.5 stock solutions. Two different proteolysis protocols were used for bottom-up proteomics of LOx samples. In the first method, the 0.2 μg/ml stock solution of trypsin protease (3 μL) was added to LOx samples in a 1:10 ratio followed by their overnight digestion at 37 °C. Digestion was stopped by acidifying samples to pH < 3.0 with 2 % formic acid. In the second method, the trypsin proteolysis as described above was followed by addition of 0.2 μg/mL stock solution of AspN protease (3 μL) to LOx samples (free form and with 800 μM Lactate) in a 1:10 ratio followed by 12-h digestion at 37 °C. Digestion was stopped by acidifying samples to pH < 3.0 with 2 % formic acid.

Digested LOx samples were diluted with 0.1 % formic acid and analyzed by a Waters nanoACQUITY UPLC coupled to a Thermo OrbitrapTM Eclipse Tribrid mass spectrometer as described earlier [47]. MassMatrix Xtreme (v3.0.10.25, MassMatrix) was used to search for unmodified and •OH labeled peptides (variable •OH modifications, no fixed modifications). Xcalibur software was used for manually extracting ion chromatograms (EIC) and analyzing the modification of LOx peptides based on MassMatrix Xtreme output. The modification extent of LOx peptides was measured by calculating the unmodified fraction as the ratio of EIC peak area of unmodified peptide to the sum of EIC peak areas of unmodified and all modified products. OriginLab software was used to generate dose-response curves by plotting the fraction of unmodified peptides vs. X-ray exposure times, and the curves were fit to a single exponential equation to calculate modification rates as described by:

$$y = exp^{-kt}$$

where k is the rate of modification in s^{-1} and t is exposure time in seconds. The observed modification rate data was converted to protection factor (PF) values for a peptide as follows,

$$PF\ (peptide) = \frac{\sum_i R_i}{k_{XFP}}$$

where R_i is the reactivity of residue i, summed over the peptide referenced to the observed peptide footprinting rate (k_{XFP}). PF values are converted to log scale (logPF) as logPF values are significantly negatively correlated to residue-weighted solvent accessibility area (SASA, $Å^2$) of a peptide [48].

The SASA values for LOx peptides were calculated as:

$$< SASA >= \frac{\sum_i R_i \times SASA_i}{\sum_i R_i}$$

Theoretical measures of solvent accessibility (SASA) for all residues in LOx for tetrameric and monomeric states were calculated using the above algorithm and the LOx crystal structure (PDB:8UFY).

2.6. Preparation of phenazine-modified mutant lactate oxidase (v3 LOx)

Phenazine-modified LOx was prepared by the following previously established protocols [15,49]. Briefly, a solution containing 6 μM of v2 LOx and 0.4 mM of activated PES (arPES) was prepared in 20 mM Tricine buffer (pH 8.3). The prepared solution was incubated at 25 °C with gentle agitation in a thermomixer for 2 h. To eliminate any unreacted arPES, the reactant was subjected to ultrafiltration at 4 °C, applying a centrifugal force of 14,000 g for durations of 5 min, and repeated across ten dilution/concentration cycles. Phosphate-buffered saline (PBS) at pH 7.0 was added prior to each ultrafiltration step to facilitate buffer exchange. The resulting phenazine-modified and histidine-tagged LOx is designated as v3 LOx herein. For comparison, v2 LOx denotes the unmodified enzyme variant without phenazine modification but with histidine-tag, whereas v1 LOx represents the histidine-tagged wild-type sequence. Prior to further experiments, all three LOx variants and commercially available LOx were adjusted to a uniform concentration of 4.5 μM in PBS.

2.7. Enzyme sensor electrode preparation

LOx-coated electrodes were prepared through the direct deposition of 10 μL of a 4.5 μM LOx stock solution onto the working electrode surface of a three-electrode, screen-printed gold electrode system. Following deposition, the electrodes with LOx application were incubated at ambient temperature for 1 h within a humidity-controlled environment to prevent the LOx solution droplet from drying. After incubation, the electrode was thoroughly washed three times with PBS to eliminate free LOx enzyme. The sensor's surface was subsequently air-dried and stored at 4 °C until use.

To confirm the successful self-immobilization of v1-v3 LOx enzymes, cyclic voltammetry (CV) and electrochemical impedance spectroscopy (EIS) were performed using a portable electrochemical analyzer, PalmSens4 (PalmSens, Inc.). Briefly, CV scans were performed using electrodes immobilized with v1-v3 LOx enzymes with 100 μL of 50 mM Sodium-L-lactate (Sigma Aldrich) in artificial sweat (Pickering Laboratories) with potential range from −0.6 V to 0.3 V at the scan rate of 100 mV/s for 20 cycles following previously established protocols. EIS were performed from 1 MHz to 0.1 Hz, at 10 mV and 8.6/dec, with 100 μL of 5 mM potassium ferricyanide/potassium ferrocyanide ($K_4[Fe(CN)_6]$) solution in 1 M potassium chloride (Sigma Aldrich).

2.8. Bare screen-printed electrode (SPE) characterization

To determine the potential difference between the reference electrode on the SPE and the standard Ag/AgCl reference electrode, the open circuit potential detection method was used. The reference and counter electrode on SPE were used as the reference and counter electrode respectively. Standard Ag/AgCl reference electrode (CH Instruments, Inc.) was used as the working electrode. The stable potential obtained by the open-circuit potential test is the difference potential (E_x) between the SPE reference electrode and the standard Ag/AgCl electrode.

2.9. Enzyme sensor characterization

To compare the performance of 3 versions of LOx, and to determine the detection voltage for the following studies, CV scans were performed using 50 mM lactate in artificial sweat, and 3 mM lactate in human serum, on sensors immobilized with v1, v2, and v3 LOx, respectively. The sweep potential for the detection test ranged from −0.1 V to 0.8 V at the scan rate of 100 mV/s for 20 cycles.

2.10. 2.10. electrochemical detection and monitoring of lactic levels

The performance of v3 LOx for lactate detection was tested in both human serum at 0.4 V vs. SPE reference electrode (0.29 V vs. standard Ag/AgCl) and artificial sweat using fast amperometry at 0.7 V vs. SPE reference electrode (0.59 V vs. standard Ag/AgCl), respectively. The performance of v3 LOx for continuous monitoring of lactate was evaluated in 75, 50, 25, and 10 mM lactate in artificial sweat using chronoamperometry, in a customized fluidic system including an InfusionONE Single Channel Syringe Pump for introducing the test lactate solution into a flow cell (Metrohm, DRP-FLWCL) that contains v3 LOx immobilized electrode.

3. Results and discussion

3.1. Biophysical and structural characterization of lactate oxidase

As part of our development of *A. viridians* LOx based lactate sensors, we wanted to ensure that our protein construct, which was evolutionarily optimized to bind lactate efficiently was fully structurally and biophysically characterized and understood in terms of substrate-binding relationships. This provides structural rationale for routes of optimization needed for specific commercial applications. The techniques used to establish this structural insight included small angle X-ray scattering and gel filtration analysis to determine distribution of oligomeric states and changes therein driven by substrate binding, a full crystallographic study in the presence of saturating concentration of lactate, and a radiolytic protein footprinting study to characterize structural dynamics and variability of ligand binding effects. While there are quite a few crystal structures of this enzyme, there are significant uncertainties as to the conformation of the dynamic loop region, residues 205–222, with multiple "choices" chosen for this region within the prior published studies. With the highest resolution structure of LOx determined to date and integrated protein biophysics measures, our

holistic structural and biophysical study provides much needed clarity as to the dynamics of this region in the protein as well as establishing our framework for sensor protein engineering.

Gel filtration and SAXS study of oligomeric state and response to substrate binding. While all structures of LOx determined to date capture the LOx oligomer as a tetramer or octamer (comprised of two pseudo-symmetric tetramers), for a durable implanted or reusable sensor module it is important to ensure that there is no loss of individual protomers during long term measurements as this would result in a loss of performance over time. Furthermore, this characterization provides a baseline characterization to which any engineered mutants can be compared to ensure that a desired oligomeric state is retained. As part of the purification of heterologously expressed LOx, we performed a gel filtration step to exchange buffer; analysis of the chromatograms and SDS PAGE studies of elution fractions during this process did not indicate any appreciable/measurable peak where a monomer or a dimer of LOx would be expected.

We also conducted small-angle X-ray scattering studies (SAXS) of LOx, which confirmed the tetrameric state as the predominant state in solution (Fig. 1A). Furthermore, comparison of SAXS profiles of lactate bound (R_g = 37.8 Å) and free (R_g = 37.9 Å) forms showed no major conformational reorganizations based on the Guinier and Distance Distribution Function (Fig. 1B–D). These observations provided certainty that in a biosensor, the leaching of monomer or other major rearrangements are not likely to occur, and that the LOx enzyme is entirely tetrameric. Interestingly, the Kratky plot shows that both LOx alone and in the presence of lactate are well folded with a certain degree of flexibility in the solution states (Fig. 1C), which may account for the differences observed in the crystal/solution structure comparisons.

Crystallographic structure determination and refinement. We employed molecular replacement to solve initial structure, using a single LOx monomer from 4RJE as a search model due to the inference in crystallographic space groups (I4 vs. C2). The initial model contained 2 copies per asymmetric unit and the crystallographic 4-fold axis recapitulated the 4-fold tetramer observed in the 4RJE model. Initial maps were subjected to automatic model building to reduce phase bias using ARP/WARP prior to hand building and model adjustment. 20 cycles of model building and refinement were performed, resulting in a 1.2 Å resolution structure (Supplementary Table 1. Summary of crystallographic data, Fig. 2, panels a,b). Due to the structural dynamics of residues 206–219, we also refined an ensemble of structures against the data using phenix_ensemble_refinement (Fig. 2, panel c). R_{work} and R_{free} improved substantially in ensemble refinement indicating that this ensemble model better fits to the structure of the protein than a single static structure. Note that the regions where loops are missing in the traditionally refined structure Fig. 2a) and b) are widely variable in the ensemble refined structure, indicating their dynamics within the structure, this correlates with their greater than expected solvent accessibility observed in the protein footprinting studies detailed below. The traditionally refined structure and data were deposited in the protein databank under accession code: 8UFY.

Radiolytic footprinting analysis to characterize dynamics of flexible regions in LOx. LOx is a large homo-tetrameric enzyme of MW 164

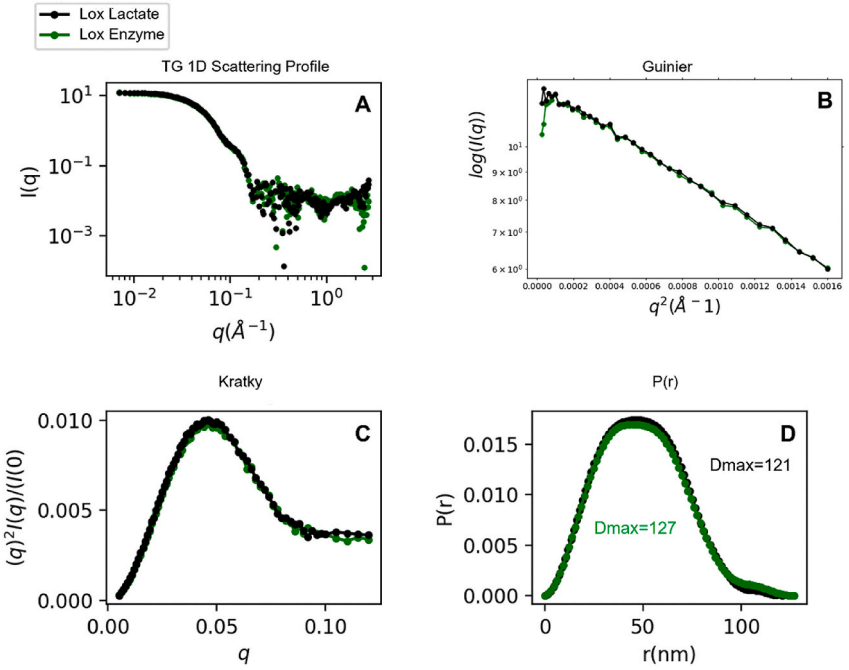

Fig. 1. SAXS data of LOx tetramer with and without lactate indicates LOx tetramer is obligate. (A) Overlay of 1D SAXS profiles show no changes in LOX tetrameric state upon addition of lactate. LOx tetramer crystal structure was superposed over SAXS derived molecular envelope (inset). **(B)** Guinier plot was used to calculate radius of gyration (R_g) and compare the size of lactate free (green, R_g = 37.9 Å) and lactate bound (black, R_g = 37.8 Å) LOx states. **(C)** Dimensionless Kratky Plot is similar in both conditions and shows some degree of flexibility in the molecule, potentially capturing the flexibility of the 205–220 loop. **(D)** Distance Distribution Function shows similar Dmax sizes and overall spherical shape.

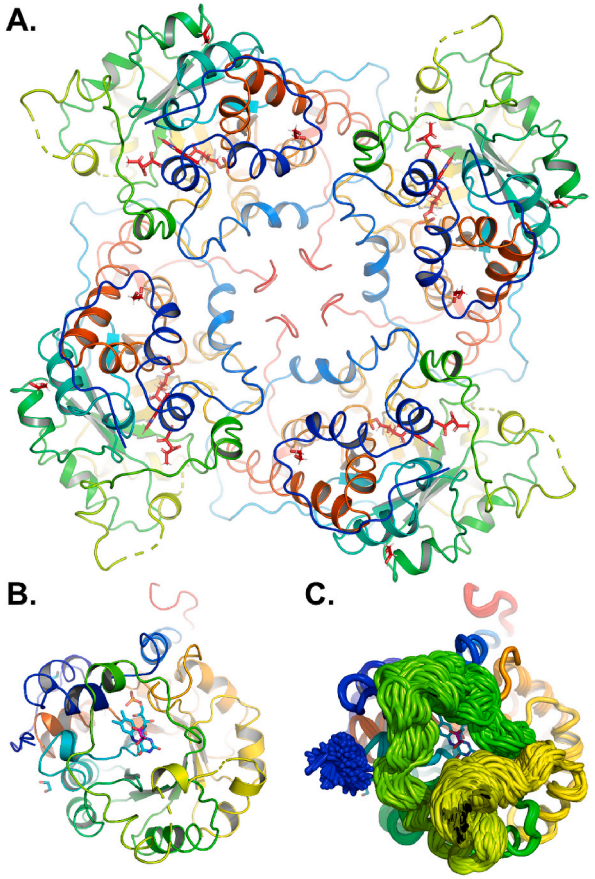

Fig. 2. Crystallographic structure of LOx. (A) The tetramer observed within the crystal structure. Note that all four N-termini (depicted in blue) are oriented in the same direction providing 24 histidine residues (four 6x His-tags) in the same locale, likely explaining why this construct can be noncovalently, but permanently linked to a rough gold substrate. Regions shown as dotted lines are disordered in the structure. **(B)** close up of the LOx monomer. Lactate entering the active site is shown in magenta. **(C)** Backbone representation of the ensemble refinement of the LOx monomer. This represents 200 models which were simultaneously refined whilst restrained against the X-ray data. Note that the two dotted regions (AAs 206–219) seen in Panels A and B are structurally the most variable, indicating their high level of structural variability.

kDa which binds a very small lactate molecule of 89 Da. Using hydroxyl radical protein footprinting (HPRF) we assessed the overall conformational changes of lactate oxidase binding to lactate in solution, in particular this was intended to provide a unique readout of the monomer/tetramer differences, probe the dynamic loop region, as well as correctly pinpoint the active site binding. HPRF studies

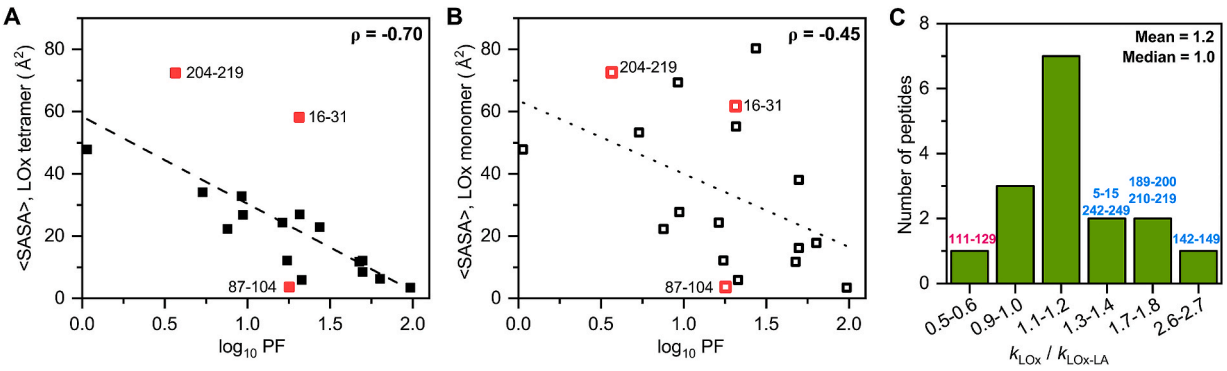

Fig. 3. X-ray footprinting results agree with a tetrameric arrangement. Correlations between the protection factors of LOx peptides (logPF) measured with XFP and the residue-weighted solvent accessibility of LOx peptides (<SASA>) for **(A)** tetramer and **(B)** monomer states. **(C)** A histogram comparing the ratios of XFP modification rates of lactate-free and lactate-bound LOx states. Pearson's coefficient (ρ) improved to ρ = −0.90 when red outlier points were removed for tetramer, while there was less improvement for monomer (ρ = −0.41).

were performed at the XFP beamline (17-BM) at the National Synchrotron Light Source II (NSLS-II). A "bottom-up" proteomics assessment was performed to quantify oxidative modifications on LOx peptides. This assessment compared the fraction of unmodified peptide to X-ray exposure time, from which we determined modification rates and the associated correlated protection factor (logPF) of LOx peptides (Supplementary Table 2). Further, Supplementary Table 2 shows the solvent accessible surface area (SASA) of each peptide for both a tetramer and monomer assumption. Fig. 3 shows plots of the measured peptide based logPF values (x-axis) vs. SASA with a tetramer assumption (Fig. 3a) compared to a monomer assumption (Fig. 3b). The logPF values of LOx peptides had a negative correlation with the SASA of the LOx tetramer ($\rho = -0.70$), while the correlation with the SASA of the LOx monomer was far lower ($\rho = -0.45$) supporting a tetramer structure assignment in solution. We observed that the theoretical SASA was higher than predicted by protection factor for two LOx segments (16–31 and 204–219). These regions are flexible in the LOx X-ray structure and their poor correlation with observed logPF values are likely due to variability of coordinates of these regions as well as reflecting potential high mobility in comparison to the rest of the tetramer.

We followed the evaluation of LOx oligomeric state by determining differences in solvent accessibility for lactate-bound and free LOx forms at a peptide level by HRPF. We calculated the ratio of OH modification rates for the free and lactate bound LOx states (Supplementary Table 3). Fig. 3C shows these data in histogram form. As lactate is ~500 times smaller in mass than LOx, the baseline expectation is that most peptides should not show much change in solvent accessibility upon lactate binding, with ratios of rates of ±lactate near 1.0. The histogram reflects this clearly, with 12 out of 16 observed peptides having ratios between 0.9 and 1.4. On the other hand, several peptides had either significant increases in ratio or were reduced significantly. Two of the highly varying peptides were in the immediate vicinity of three highly mobile regions (111–129, ratio = 0.5; 189–200, ratio = 1.7; 210–219 ratio = 1.4) of the LOx crystal structure indicating that lactate binding changes the conformation of these regions, specifically in a loop that caps the FMN cofactor and lactate substrate site. Further, the protection of 2.6-fold for peptide 142–149 properly reflects lactate direct binding at this site. Overall, these structural analyses provide a solid framework for analyzing the performance of the variants in actual sensing applications.

3.2. Determination of SPE reference electrode potential

The potential difference (E_x) between the standard Ag/AgCl reference electrode and the SPE reference electrode is determined to be −0.11V (Fig. S1). Since the actual potential of a standard Ag/AgCl electrode is 0.197 V, the potential of the SPE reference electrode

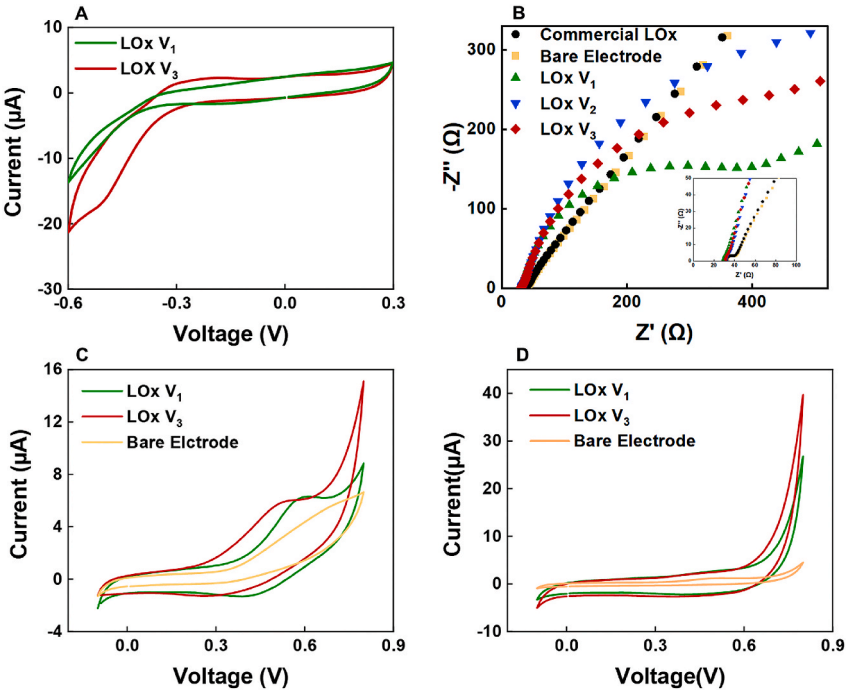

Fig. 4. Characterization of electrochemical properties of electrode immobilized with LOx variants. (A) Cyclic voltammetry results of v1 and v3 LOx modified electrodes. The significantly altered redox peak compared to wt LOx (v1) indicated successful modification of phenazine on v3 LOx. **(B)** Electrochemical impedance spectroscopy results of bare electrode, v1-v3 LOx modified electrodes, and electrode "modified" with commercial LOx. The inset demonstrates a magnified view of the high-frequency regions. Electrode treated with commercial (non-his-tagged) LOx is indistinguishable from **(C, D)** Cyclic voltammetry results generated using bare electrode, and electrodes immobilized with wildtype LOx (v1) and v3 LOx for the detecting 3 mM lactate in human serum **(C)** and 50 mM lactate in artificial sweat **(D)**. Phenazine modification improves the electron transfer ability of v3 LOx and thus reduces the lactate operating in both human serum and artificial sweat, compared to the wildtype LOx (v1).

can be determined by E_x = 0.197 – x, thus x = 0.308 V is the actual potential of the SPE reference electrode. In this manuscript, all reported voltages are referenced against the SPE reference electrode. Therefore, unless otherwise specified, the applied voltages relative to the standard Ag/AgCl reference electrode can be obtained by adjusting the voltages measured against the SPE reference electrode by subtracting 0.11 V.

3.3. Electrochemical characterization of LOx modification and self-immobilization

3.3.1. Cyclic voltammetry characterization of phenazine–modified LOx

CV tests were conducted to confirm the successful modification by PES, resulting in the formation of v3 LOx. The CV test results (Fig. 4A) exhibited a redox peak between −0.3 V and −0.5 V only for phenazine-modified LOx (v3), but not for wild type LOx (v1). This result agrees with the prior research indicating that phenazine-modified LOx exhibits redox activity within this voltage window [15]. As a result, the presence of this redox peak conclusively confirmed the effective phenazine modification, thereby producing v3 LOx.

3.3.2. Electrochemical impedance spectroscopy characterization of LOx self-immobilization (***Hexahistidine tag is both necessary and sufficient for immobilization***)

The LOx self-immobilization mechanism is evaluated using EIS studies, which is based on electron transfer resistance. In the EIS curve, the semicircle diameter and the slope of the linear portion are correlated to the charge transfer resistance and diffusion process, respectively [50,51]. In this work, EIS tests were performed using 5 mM potassium ferricyanide/potassium ferrocyanide (K_3[Fe

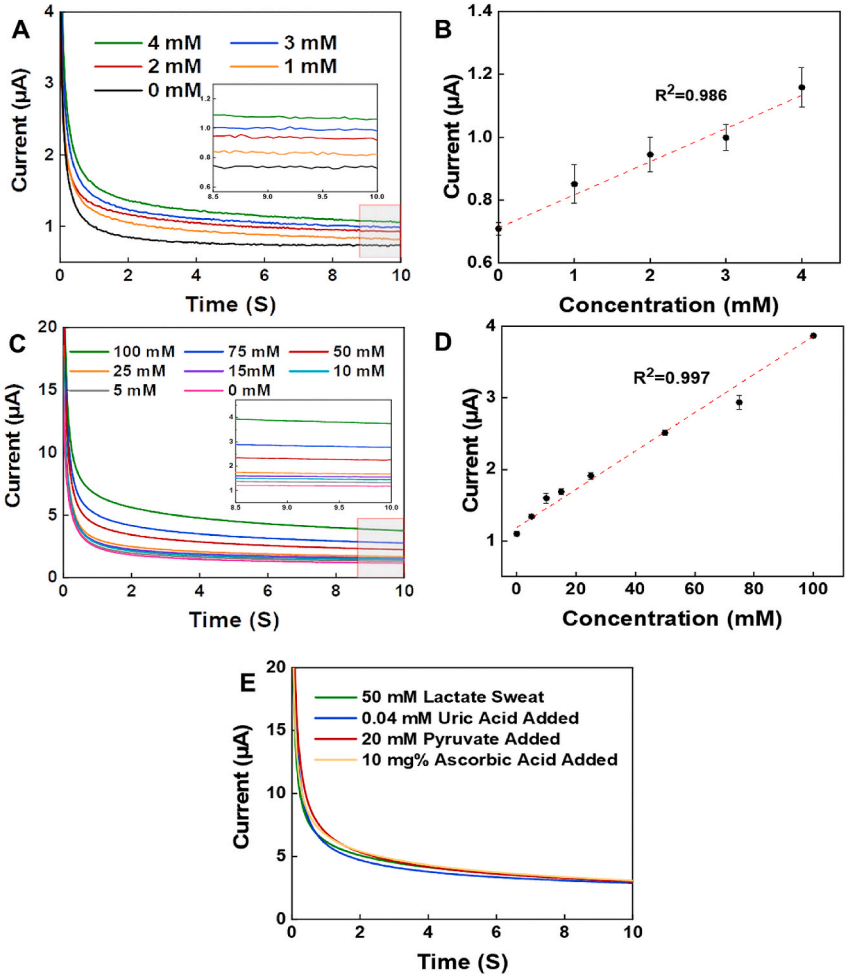

Fig. 5. Results from rapid amperometry testing for lactate detection in human serum and artificial sweat with electrodes immobilized with v3 LOx. **(A)** Lactate detection in human serum at 0, 1, 2, 3, and 4 mM. **(B)** The steady-state current recorded across a range of lactate concentrations in serum exhibited strong linearity ($R^2 = 0.986$). **(C)** Lactate detection in artificial sweat at 0, 1, 2, 3, and 4 mM. **(D)** The steady-state current recorded across a range of lactate concentrations in artificial sweat exhibited strong linearity ($R^2 = 0.997$). **(E)** Anti-interference tests of electrodes immobilized with v3 LOx. The addition of 0.04 mM uric acid, 20 mM pyruvate, and 10 mg/L ascorbic acid did not significantly change the response current. (error bars in B&D indicate standard deviation, n = 3).

$(CN)_6]/K_4[Fe(CN)_6]$) solution in 1 M KCl. The Nyquist diagram of v1 (green), v2 (blue), and v3 (red) LOx all exhibit larger semicircles compared to the bare electrode without enzyme immobilization (brown), and compared to the electrode incubated with commercial LOx (black) under higher frequency ranges (Fig. 4B, semicircles were shown in the inset figure). These results demonstrated that all 3 versions of customized LOx, but not commercial LOx, were successfully immobilized onto working electrodes through self-immobilization without the need for any covalent treatment,. Comparative analysis of the semicircle diameters in the middle and high frequency regions reveals that the order of diameters for the LOx-modified electrodes is v2 > v1 > v3. The reduced diameter observed in electrodes modified with v3 LOx, as opposed to those modified with v1 and v2 LOx, is likely attributable to the presence of phenazine molecules, which may enhance the rate of electron transfer. Finally, the linear portion of all electrode readouts exhibit a similar slope, indicating that the LOx modification did not affect the rates of ion diffusion to electrode surfaces.

3.4. Cyclic voltammetry characterization of phenazine -modification of v3 LOx in lactate electrochemical sensing

Under physiological conditions, lactate levels in human blood range from 0.5 to 2.2 mM, with levels exceeding 2.2 mM potentially signaling conditions including hypoxia or lactic acidosis, and with critical concern above 4 mM. Meanwhile, physiological lactate concentrations in sweat fall between 5 and 25 mM but can escalate to 43.7 mM during endurance exercise and peak at 115.8 mM in scenarios of exhaustive exercise [24,25]. The performance of v1 (wildtype LOx), and v3 (phenazine-modified LOx) enzymes were evaluated and compared using CV tests at elevated lactate levels of 50 mM in artificial sweat (Fig. 4C) and 3 mM in human serum (Fig. 4D). In human serum, electrodes immobilized with v3 LOx exhibited an oxidation peak at decreased voltage of 0.525 V vs. SPE reference electrode, compared to the v1 LOx oxidation peak at 0.600 V. Based on these CV results and our extensive experimental tests, 0.4 V vs. SPE reference electrode (0.29 V vs. standard Ag/AgCl electrode) was selected in the subsequent lactate sensing tests in serum. In artificial sweat, electrodes immobilized with v3 LOx exhibited increased current response compared to the ones immobilized with v1 LOx at 0.6–0.8 V vs. SPE reference electrode. Based on these CV results, 0.7 V vs. SPE reference electrode (0.59 V vs. standard Ag/AgCl electrode) was selected in the subsequent lactate sensing tests in artificial sweat. Together, these results demonstrated that v3 LOx with phenazine modification indeed improved lactate detection sensitivity compared to wildtype LOx, in both human serum and artificial sweat. However, the underlying mechanism of the role of phenazine in mediating lactate sensing at 0.29 V in human serum and at 0.59 V in artificial sweat remains unclear, as this does not appear to be the result of direct electron measurement at the electrode surface.

3.5. Fast amperometry characterization of v3 LOx in lactate detection

The performance of v3 LOx in detecting lactate in human serum (0, 1, 2, 3, and 4 mM, Fig. 5A&B) and in artificial sweat (0, 5, 10, 15, 25, 50, 75, and 100 mM, Fig. 5C&D) were tested using fast amperometry at 0.4 and 0.7 V vs. SPE reference electrode (0.29 V and 0.59 V vs. standard Ag/AgCl), respectively. These concentrations of lactate mimic physiological levels of lactate in serum during hypoxia or lactic acidosis, and in sweat during endurance and exhaustive exercises. The amperometric response observed in human serum indicates a linear increase in current with rising lactate concentrations. For the electrode modified with v3 LOx, the sensitivity to lactate in sweat was determined to be 0.106 μA/mM. The relationship is best described by the linear equation $y = 0.106x + 0.711$, where the coefficient of determination (R^2) for this linear fit is 0.986 (Fig. 5A&B). Similarly, the sensitivity to lactate in sweat was determined to be 0.027 μA/mM and the relationship is best described by the linear equation $y = 0.027x + 1.187$, with R^2 of 0.997 (Fig. 5C&D). These findings highlight that the v3 LOx-modified sensors exhibit a robust linear response in detecting lactate in both sweat and serum/blood, suggesting its applicability over a broad spectrum of physiologically relevant lactate concentrations.

The selectivity of the v3 LOx sensor is determined from the interference experiments (Fig. 5E). These experiments involved measuring the sensor's current response to a constant lactate concentration while introducing other sweat metabolites including 0.04

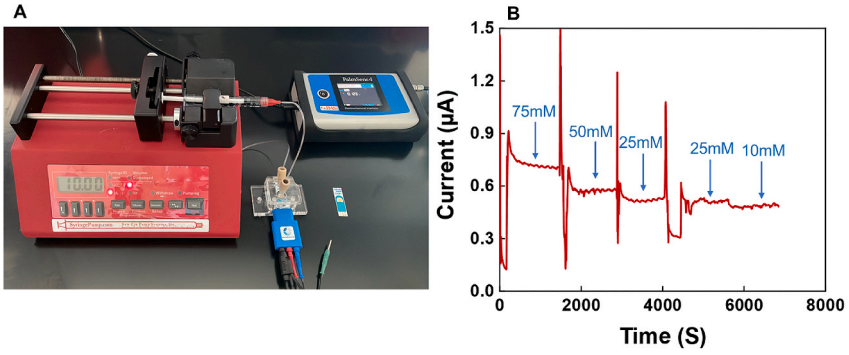

Fig. 6. Continuous measurement of lactate in a flow cell based device.(A) Fluidic flow-based system enabling lactate continuous monitoring under continuous fluid flow. **(B)** Chronoamperometry results revealed the functionality and stability of v3 LOx in continuous lactate monitoring in artificial sweat under continuous flow over a 2 h test period. Current fluctuations across varying concentrations were attributed to flow disturbances triggered by the transition between solutions.

mM uric acid, 20 mM pyruvate, and 10 mg/L ascorbic acid. An optimal sensor would exhibit minimal current fluctuation with the addition of each metabolite, a characteristic observed with the v3 LOx sensor in Fig. 5E. Notably, uric acid and ascorbic acid were tested due to their low oxidation potentials, whereas pyruvate was included for its structural resemblance to lactate and potential for product inhibition. The outcomes of these tests confirm that the v3 LOx sensor maintains its high selectivity for lactate.

3.6. Chronoamperometry characterization of v3 LOx in lactate monitoring

Continuous monitoring of lactate levels is crucial for real-time assessment of metabolic status and early detection of imbalances, significantly impacting patient care and management. Chronoamperometry was conducted within a continuous flow system to test the performance of v3 LOx in continuous monitoring using a range of lactate concentrations in artificial sweat (Fig. 6A). The sample flows over the surface of the sensing area at a rate of 100 μL/min. Our test results revealed the functionality and stability of v3 LOx in continuous lactate monitoring under fluid flow over a 2-h test period in a range of lactate concentrations ranging from 75, 50, 25, and 10 mM. These concentrations were selected to reflect both physiological conditions and conditions during endurance and exhaustive exercises. Continuous monitoring across a range from high to low lactic acid concentrations serves to demonstrate the sensor's stability during extended test time of 2 h (Fig. 6B). The fluctuations in current are caused by flow disturbances that occurred during the exchange of solutions with varying lactate concentrations. Additionally, the relaxation time, i.e., duration for current to reach a steady state, is due to the time required to fully replace the previous solution with the next solution.

4. Conclusion

By various modifications of lactate oxidase, we engineered an optimized self-immobilizable LOx variant v3. Due to its phenazine modification, v3 LOx has excellent electron transport capability, which can significantly reduce the detection potential for lactate. Based upon electrochemical characterization, the v3 LOx immobilized electrode shows the best sensitivity and stability among three tested LOx electrode versions. The v3 LOx electrode can be used to detect lactate in a complex environment of sweat and serum with sensitivities of 0.027 μA/mM in sweat and 0.106 μA/mM in blood. Further, v3 LOx shows good stability and repeatability in continuous monitoring of flowing liquid samples over a period of more than 2 h. Overall, our results demonstrate that v3 LOx -modified lactic acid sensor can be used for continuous monitoring in complex environments such as sweat and serum. Our integrated structure-bioengineering approach to utilizing protein biophysics at the outset of this sensor design project provided structural, dynamic and functional data to springboard sensor design optimized to the application needed. Further, this approach is not limited to enzyme or even peptide-based modules as nucleic acid aptamers or other engineered binding elements are likewise amenable to high-resolution structural and dynamic characterization to provide the foundation for directed and "fit-for-purpose" sensor development.

Disclaimer

This material is based on research sponsored by AFRL under agreement number FA8650-18-2-5402 (Case Number AFRL 2024-1441). The U.S. Government is authorized to reproduce and distribute reprints for Government purposes notwithstanding any copyright notation thereon. The views and conclusions contained herein are those of the authors and should not be interpreted as necessarily representing the official policies or endorsements, either expressed or implied, of AFRL or the U.S. Government.

CRediT authorship contribution statement

Qingrong He: Data curation, Formal analysis, Methodology, Visualization, Writing – original draft. **Cheng Wang:** Data curation, Formal analysis, Validation, Writing – original draft. **Rohit Jain:** Data curation, Formal analysis, Methodology, Visualization, Writing – original draft, Writing – review & editing. **James Byrnes:** Data curation, Formal analysis, Visualization, Writing – original draft, Writing – review & editing. **Erik R. Farquhar:** Data curation, Formal analysis, Methodology, Supervision, Writing – review & editing. **Elliot Reed:** Conceptualization, Funding acquisition, Supervision, Writing – review & editing. **Elizabeth Berezovsky:** Conceptualization, Methodology, Supervision, Writing – review & editing. **Mark R. Chance:** Conceptualization, Funding acquisition, Methodology, Supervision, Writing – review & editing. **David Lodowski:** Conceptualization, Data curation, Funding acquisition, Methodology, Project administration, Supervision, Writing – original draft, Writing – review & editing. **Ran An:** Conceptualization, Data curation, Resources, Supervision, Writing – original draft, Writing – review & editing.

Declaration of competing interest

The authors disclose that a provisional patent application related to the findings of this paper has been filed by Ran An, David Lodowski, and Mark Chance.

Acknowledgments

This research was supported by the National Institutes of Health under R01-GM141078 and the Air Force Research Laboratory under agreement number FA8650-18-2-5402 (Case Number AFRL-pending). This research used the 16-ID (LiX) and 17-BM (XFP) and 17-ID-1 (AMX) beamlines of the NSLS-II, a U.S. DOE Office of Science User Facility operated for the DOE Office of Science by

Brookhaven National Laboratory under Contract No. DE-SC0012704. Funding for development of the XFP beamline was provided by a Major Research Instrumentation award from the NSF (DBI-1228549) and Case Western Reserve University. The LiX and AMX beamlines are part of the Center for BioMolecular Structure (CBMS), which is primarily supported by the National Institutes of Health, National Institute of General Medical Sciences (NIGMS) through a P30 Grant (P30-GM133893),and by the DOE Office of Biological and Environmental Research (KP1605010). LiX also received additional support from NIH Grant S10 OD012331. This work is based upon research conducted at the Northeastern Collaborative Access Team beamlines, which are funded by the National Institute of General Medical Sciences from the National Institutes of Health (P30 GM124165). This research used resources of the Advanced Photon Source, a U.S. Department of Energy (DOE) Office of Science User Facility operated for the DOE Office of Science by Argonne National Laboratory under Contract No. DE-AC02-06CH11357. The DOE has established a portal for accessing X-ray footprinting beamlines at: https://berstructuralbioportal.org/x-ray-footprinting/

Appendix A. Supplementary data

Supplementary data to this article can be found online at https://doi.org/10.1016/j.heliyon.2024.e34301.

References

[1] M.A. Komkova, A.A. Eliseev, A.A. Poyarkov, E.V. Daboss, P.V. Evdokimov, A.A. Eliseev, A.A. Karyakin, Simultaneous monitoring of sweat lactate content and sweat secretion rate by wearable remote biosensors, Biosens. Bioelectron. 202 (2022) 113970.
[2] K.-C. Lin, S. Muthukumar, S. Prasad, Flex-GO (Flexible graphene oxide) sensor for electrochemical monitoring lactate in low-volume passive perspired human sweat, Talanta 214 (2020) 120810.
[3] X. Li, Y. Yang, B. Zhang, X. Lin, X. Fu, Y. An, Y. Zou, J.-X. Wang, Z. Wang, T. Yu, Lactate metabolism in human health and disease, Signal Transduct. Targeted Ther. 7 (1) (2022) 305.
[4] D. Jiang, C. Xu, Q. Zhang, Y. Ye, Y. Cai, K. Li, Y. Li, X. Huang, Y. Wang, In-situ preparation of lactate-sensing membrane for the noninvasive and wearable analysis of sweat, Biosens. Bioelectron. 210 (2022) 114303.
[5] N.V. Zaryanov, V.N. Nikitina, E.V. Karpova, E.E. Karyakina, A.A. Karyakin, Nonenzymatic sensor for lactate detection in human sweat, Anal. Chem. 89 (21) (2017) 11198–11202.
[6] S. Kushimoto, S. Akaishi, T. Sato, R. Nomura, M. Fujita, D. Kudo, Y. Kawazoe, Y. Yoshida, N. Miyagawa, Lactate, a useful marker for disease mortality and severity but an unreliable marker of tissue hypoxia/hypoperfusion in critically ill patients, Acute Med Surg 3 (4) (2016) 293–297.
[7] R. Beneke, R.M. Leithäuser, O. Ochentel, Blood lactate diagnostics in exercise testing and training, Int. J. Sports Physiol. Perform. 6 (1) (2011) 8–24.
[8] S. Campuzano, M. Pedrero, P. Yáñez-Sedeño, J.M. Pingarrón, New challenges in point of care electrochemical detection of clinical biomarkers, Sensor. Actuator. B Chem. 345 (2021) 130349.
[9] C. Wang, M. Liu, Z. Wang, S. Li, Y. Deng, N. He, Point-of-care diagnostics for infectious diseases: from methods to devices, Nano Today 37 (2021) 101092.
[10] C. Wang, R. Wu, L. Wang, X. Wang, Multifunctional flexible graphene oxide/bacterial cellulose composite paper platforms for realtime monitoring sweat and strain in wearable devices, Chem. Eng. J. 481 (2024) 148390.
[11] F. Alam, S. RoyChoudhury, A.H. Jalal, Y. Umasankar, S. Forouzanfar, N. Akter, S. Bhansali, N. Pala, Lactate biosensing: the emerging point-of-care and personal health monitoring, Biosens. Bioelectron. 117 (2018) 818–829.
[12] M. Regiart, A. Ledo, E. Fernandes, G.A. Messina, C.M.A. Brett, M. Bertotti, R.M. Barbosa, Highly sensitive and selective nanostructured microbiosensors for glucose and lactate simultaneous measurements in blood serum and in vivo in brain tissue, Biosens. Bioelectron. 199 (2022) 113874.
[13] Y. Zhang, L. Xu, J. Ge, Multienzyme system in Amorphous metal–organic frameworks for intracellular lactate detection, Nano Lett. 22 (12) (2022) 5029–5036.
[14] A. Patgiri, O.S. Skinner, Y. Miyazaki, G. Schleifer, E. Marutani, H. Shah, R. Sharma, R.P. Goodman, T.L. To, X. Robert Bao, F. Ichinose, W.M. Zapol, V.K. Mootha, An engineered enzyme that targets circulating lactate to alleviate intracellular NADH:NAD(+) imbalance, Nat. Biotechnol. 38 (3) (2020) 309–313.
[15] K. Hiraka, K. Kojima, W. Tsugawa, R. Asano, K. Ikebukuro, K. Sode, Rational engineering of Aerococcus viridans l-lactate oxidase for the mediator modification to achieve quasi-direct electron transfer type lactate sensor, Biosens. Bioelectron. 151 (2020) 111974.
[16] X. Xuan, C. Pérez-Ràfols, C. Chen, M. Cuartero, G.A. Crespo, Lactate biosensing for reliable on-body sweat analysis, ACS Sens. 6 (7) (2021) 2763–2771.
[17] W. Gao, X. Zhou, N.F. Heinig, J.P. Thomas, L. Zhang, K.T. Leung, Nonenzymatic saliva-range glucose sensing using electrodeposited cuprous oxide nanocubes on a graphene strip, ACS Appl. Nano Mater. 4 (5) (2021) 4790–4799.
[18] Z. Altintas, M. Akgun, G. Kokturk, Y. Uludag, A fully automated microfluidic-based electrochemical sensor for real-time bacteria detection, Biosens. Bioelectron. 100 (2018) 541–548.
[19] T. Yang, R. Yu, Y. Yan, H. Zeng, S. Luo, N. Liu, A. Morrin, X. Luo, W. Li, A review of ratiometric electrochemical sensors: from design schemes to future prospects, Sensor. Actuator. B Chem. 274 (2018) 501–516.
[20] J. Ding, X. Li, L. Zhou, R. Yang, F. Yan, B. Su, Electrodeposition of nickel nanostructures using silica nanochannels as confinement for low-fouling enzyme-free glucose detection, J. Mater. Chem. B 8 (16) (2020) 3616–3622.
[21] B.T.P. Quynh, J.Y. Byun, S.H. Kim, Non-enzymatic amperometric detection of phenol and catechol using nanoporous gold, Sensor. Actuator. B Chem. 221 (2015) 191–200.
[22] N.T. Garland, J. Schmieder, Z.T. Johnson, R.G. Hjort, B. Chen, C. Andersen, D. Sanborn, G. Kjeldgaard, C.C. Pola, J. Li, C. Gomes, E.A. Smith, H. Angus, J. Meyer, J.C. Claussen, Wearable flexible perspiration biosensors using laser-induced graphene and polymeric tape microfluidics, ACS Appl. Mater. Interfaces 15 (32) (2023) 38201–38213.
[23] Y. Jiang, Y. Yang, L. Shen, J. Ma, H. Ma, N. Zhu, Recent advances of prussian blue-based wearable biosensors for healthcare, Anal. Chem. 94 (1) (2022) 297–311.
[24] P.J. Derbyshire, H. Barr, F. Davis, S.P.J. Higson, Lactate in human sweat: a critical review of research to the present day, J. Physiol. Sci. 62 (6) (2012) 429–440.
[25] K. Mitsubayashi, M. Suzuki, E. Tamiya, I.J. A.c. a. Karube, Analysis of metabolites in sweat as a measure of physical condition 289 (1) (1994) 27–34.
[26] N. Plumeré, Interferences from oxygen reduction reactions in bioelectroanalytical measurements: the case study of nitrate and nitrite biosensors, Anal. Bioanal. Chem. 405 (11) (2013) 3731–3738.
[27] S.F. Cogan, J. Ehrlich, T.D. Plante, M.D. Gingerich, D.B. Shire, Contribution of oxygen reduction to charge injection on platinum and sputtered iridium oxide neural stimulation electrodes, IEEE Trans. Biomed. Eng. 57 (9) (2010) 2313–2321.
[28] J. Kim, S. Park, H. Yang, Wash-free photoelectrochemical DNA detection based on photoredox catalysis combined with electroreduction and light blocking by magnetic microparticles, Talanta 253 (2023) 123872.
[29] C.S. Pundir, V. Narwal, B. Batra, Determination of lactic acid with special emphasis on biosensing methods: a review, Biosens. Bioelectron. 86 (2016) 777–790.
[30] V.P. Zanini, B. López de Mishima, V. Solís, An amperometric biosensor based on lactate oxidase immobilized in laponite–chitosan hydrogel on a glassy carbon electrode. Application to the analysis of l-lactate in food samples, Sensor. Actuator. B Chem. 155 (1) (2011) 75–80.

[31] B. Lillis, C. Grogan, H. Berney, W.A. Lane, Investigation into immobilisation of lactate oxidase to improve stability, Sensor. Actuator. B Chem. 68 (1) (2000) 109–114.
[32] M. Trojanowicz, O. Geschke, T.K. vel Krawczyk, K.J.S. Cammann, A.B. Chemical, Biosensors based on oxidases immobilized in various conducting polymers 28 (3) (1995) 191–199.
[33] F. Palmisano, M. Quinto, R. Rizzi, P.G. Zambonin, Flow injection analysis of L-lactate in milk and yoghurt by on-line microdialysis and amperometric detection at a disposable biosensor, The Analyst 126 (6) (2001) 866–870.
[34] M. Gamero, F. Pariente, E. Lorenzo, C. Alonso, Nanostructured rough gold electrodes for the development of lactate oxidase-based biosensors, Biosens. Bioelectron. 25 (9) (2010) 2038–2044.
[35] F. Palmisano, R. Rizzi, D. Centonze, P.G. Zambonin, Simultaneous monitoring of glucose and lactate by an interference and cross-talk free dual electrode amperometric biosensor based on electropolymerized thin films, Biosens. Bioelectron. 15 (9) (2000) 531–539.
[36] A. Silvestri, F. Wang, X. Feng, A.L. Cortajarena, M. Prato, Protein-based (bio)materials: a way toward high-performance graphene enzymatic biosensors, J. Mater. Chem. C 10 (14) (2022) 5466–5473.
[37] F. Alam, A.H. Jalal, S. Forouzanfar, M. Karabiyik, A.R. Baboukani, N. Pala, Flexible and linker-free enzymatic sensors based on zinc oxide nanoflakes for noninvasive L-lactate sensing in sweat, IEEE Sensor. J. 20 (10) (2020) 5102–5109.
[38] O. Domínguez-Renedo, A.M. Navarro-Cuñado, M.A. Alonso-Lomillo, Recent trends in enzyme-based electrosensing devices modified with nanomaterials, in: B. Purohit, P. Chandra (Eds.), Surface Engineering and Functional Nanomaterials for Point-of-Care Analytical Devices, Springer Nature Singapore, Singapore, 2023, pp. 223–257.
[39] J.S. Narayanan, G. Slaughter, Lactic acid biosensor based on lactate dehydrogenase immobilized on Au nanoparticle modified microwire electrode, IEEE Sensor. J. 20 (8) (2020) 4034–4040.
[40] P. Samadi Pakchin, H. Ghanbari, R. Saber, Y. Omidi, Electrochemical immunosensor based on chitosan-gold nanoparticle/carbon nanotube as a platform and lactate oxidase as a label for detection of CA125 oncomarker, Biosens. Bioelectron. 122 (2018) 68–74.
[41] A. Parra, E. Casero, L. Vázquez, F. Pariente, E. Lorenzo, Design and characterization of a lactate biosensor based on immobilized lactate oxidase onto gold surfaces, Anal. Chim. Acta 555 (2) (2006) 308–315.
[42] L. Yang, S. Antonelli, S. Chodankar, J. Byrnes, E. Lazo, K.J. J.o.S.R. Qian, Solution scattering at the life science X-ray scattering (LiX) beamline 27 (3) (2020) 804–812.
[43] L. Yang, E. Lazo, J. Byrnes, S. Chodankar, S. Antonelli, M. Rakitin, Tools for supporting solution scattering during the COVID-19 pandemic 28 (4) (2021) 1237–1244.
[44] K. Manalastas-Cantos, P.V. Konarev, N.R. Hajizadeh, A.G. Kikhney, M.V. Petoukhov, D.S. Molodenskiy, A. Panjkovich, H.D. Mertens, A. Gruzinov, C.J. J.o. a. c. Borges, Atsas 3.0: expanded functionality and new tools for small-angle scattering data analysis 54 (1) (2021) 343–355.
[45] R. Jain, D. Abel, M. Rakitin, M. Sullivan, D.T. Lodowski, M.R. Chance, E. Farquhar, New high-throughput endstation to accelerate the experimental optimization pipeline for synchrotron X-ray footprinting 28 (5) (2021) 1321–1332.
[46] E.R. Farquhar, K. Vijayalakshmi, R. Jain, B. Wang, J. Kiselar, M.R.J.B. Chance, B.R. Communications, Intact Mass Spectrometry Screening to Optimize Hydroxyl Radical Dose for Protein Footprinting, 2023.
[47] R. Jain, N.S. Dhillon, V.L. Kanchustambham, D.T. Lodowski, E.R. Farquhar, J. Kiselar, M.R. Chance, Evaluating mass spectrometry-based hydroxyl radical protein footprinting of a benchtop flash oxidation system against a synchrotron X-ray beamline, J. Am. Soc. Mass Spectrom. 35 (3) (2024) 476–486. https://pubs.acs.org/doi/10.1021/jasms.3c00368.
[48] W. Huang, Krishnakumar M. Ravikumar, Mark R. Chance, S. Yang, Quantitative mapping of protein structure by hydroxyl radical footprinting-mediated structural mass spectrometry: a protection factor analysis, Biophys. J. 108 (1) (2015) 107–115.
[49] M. Hatada, N. Loew, Y. Inose-Takahashi, J. Okuda-Shimazaki, W. Tsugawa, A. Mulchandani, K. Sode, Development of a glucose sensor employing quick and easy modification method with mediator for altering electron acceptor preference, Bioelectrochemistry 121 (2018) 185–190.
[50] C. Wang, Z. Zhao, R. Wu, X. Shi, G.F. Payne, X. Wang, Fabrication of robust paper-based electronics by adapting conventional paper making and coupling with wet laser writing, ACS Sustain. Chem. Eng. 11 (26) (2023) 9782–9791.
[51] L. Chen, Y. Gao, Y. Li, C. Wang, D. Chen, Y. Gao, X.J.N. Ran, s. o. sleep, Severe Intermittent Hypoxia Modulates the Macrophage Phenotype and Impairs Wound Healing through Downregulation of HIF-2α, 2022, pp. 1511–1520.